Resonant attenuation of acoustic phonons in metallic superlattices

2002 J. Phys.: Condens. Matter 14 689

(http://iopscience.iop.org/0953-8984/14/4/304)

INSTITUTE OF PHYSICS PUBLISHING JOURNAL OF PHYSICS: CONDENSED MATTER

J. Phys.: Condens. Matter **14** (2002) 689–702 PII: S0953-8984(02)31300-6

Resonant attenuation of acoustic phonons in metallic superlattices

S Tamura[1] **and N Perrin**[2]

[1] Department of Applied Physics, Hokkaido University, Sapporo 060-8628, Japan
[2] Laboratoire de Physique de la Matière Condensée de l'Ecole Normale Superieure, 24 rue Lhomond, 75231 Paris Cédex 5, France

Received 19 November 2001
Published 18 January 2002
Online at stacks.iop.org/JPhysCM/14/689

Abstract

The attenuation rate of high-frequency sound waves (phonons) in a bulk metal was calculated by Pippard assuming the free-electron model and the deformation-potential coupling of the electron–phonon interaction. We study the correction to the Pippard theory in a metallic superlattice. A remarkable feature that we predict is the existence of the resonant absorption of the phonons by electrons. This happens due to the alteration of the band structures of electrons arising from their Brillouin-zone folding.

1. Introduction

The attenuation rate of high-frequency sound (longitudinal phonons) in bulk metals was calculated by Pippard many years ago [1, 2]. Pippard assumed the free-electron model of the metal and the deformation-potential coupling of the electron–phonon interaction. According to his result, the attenuation rate τ^{-1} (τ is the relaxation time) increases in proportion to the ultrasound frequency, and is given by the Pippard formula:

$$\tau^{-1} = \frac{C^2 m^2}{2\pi\hbar^3 \rho v}\omega \tag{1}$$

where C is the deformation potential, m is the free-electron mass, ρ is the mass density of the metal, v is the longitudinal sound velocity, and ω is the angular frequency. This result was proved experimentally by Hepfer and Rayne [3] for aluminium, though a slight anisotropy has been observed depending on the propagation direction.

Recently, a considerable number of studies have been made on the acoustic wave propagation in multilayered elastic systems, or superlattices. The folding of acoustic band structure and the opening of new gaps in superlattices have now been known of for a long time [4–7]. Moreover, in a semi-infinite superlattice with the free surface, the existence of vibrations or acoustic waves localized at a free surface has been reported [8–14]. These surface vibrations, or surface phonons, may appear within the extra gaps that exist between the folded bulk bands and they depend on the kind of layer that is near the surface. Recently, with the use

of picosecond ultrasonics, Chen *et al* [15] observed, in Al/Ag superlattices, lattice vibrations that remain near to the free surface for longer than 200 ps. The frequencies of these surface vibrations (surface phonons) coincide well with the values predicted by theory taking account of the internal structure of a unit period. The damping rates of these surface phonons are also measured and found to vary linearly with frequency (in the range 100–300 GHz for various bilayer thicknesses) but to be nearly independent of temperature from 70 to 300 K.

This variation of the attenuation with frequency suggests that it is due to an interaction between high-frequency phonons and electrons, as in Pippard's theory for the attenuation of longitudinal sound waves in bulk metals [1]. However, there is a quantitative discrepancy between the measured attenuation rate and the values expected from Pippard theory: that is, the magnitude of the measured damping is about three times and approximately 25 times larger than the values expected for bulk aluminium and silver respectively. According to the Pippard formula, the damping rate in Al is, thus, about one order of magnitude larger than the damping rate in Ag. Hence, a larger damping would be expected in superlattices that contain a larger volume of Al. In fact, the samples studied by Chen *et al* with different ratios (<1 or >1) of the Al thickness to the Ag thickness do not exhibit significant change of the attenuation rate, suggesting an enhanced scattering in the Ag layer.

Here it should be noted that the Pippard formula gives the attenuation of sound by free electrons in bulk metals, and so we can suppose that the attenuation is increased because of the effects of the band structures of both the phonons and electrons in superlattices as was suggested by Chen *et al* [15]. Moreover, we may wonder whether the apparently enhanced scattering in the Ag layers also results from the folded band structures. However, up to now no theoretical study has been made to resolve these points.

The purpose of this paper, therefore, is to study the correction to the Pippard formula for the attenuation of bulk longitudinal phonons due to the folded band structure in metallic superlattices. More specifically, our model takes account of: (1) a Kronig–Penney model for electrons; (2) the continuum elasticity theory for acoustic phonons in superlattices; and (3) the deformation-potential coupling for the electron–phonon interaction. A remarkable result that we will predict is the existence of resonant phonon absorption by electrons, which does not occur in bulk metals. This is mainly due to the alteration of the band structures of the electrons, and independent of the details of the electron–phonon interaction.

In the next section, we recapitulate the derivation of acoustic dispersion relations for superlattices. Also explicit expressions are given for the displacement fields of phonons. The electron fields in the Kronig–Penney models are given in section 3. In section 4 the electron–phonon interaction is formulated, and the resulting expressions for the scattering rates of phonons are derived in section 5. The numerical calculations of the attenuation rates in Al/Ag superlattices are developed in section 6. Concluding remarks are given in section 7.

2. Phonons in superlattices: quantized displacement

We consider a periodic superlattice consisting of alternating A and B layers with layer thickness d_A and d_B (the unit period, or bilayer thickness is $D = d_A + d_B$), densities ρ_A and ρ_B, and sound velocities v_A and v_B, respectively. The layer interfaces of the superlattice are taken to be parallel to the $\boldsymbol{x}_\parallel = (x, y)$ plane and the growth direction is parallel to the z-direction.

In this work we study the longitudinal phonons propagating in the z-direction perpendicular to the layer interfaces, i.e., $\boldsymbol{k}_\parallel = 0$, where $\boldsymbol{k}_\parallel$ is the two-dimensional wavevector in the $\boldsymbol{x}_\parallel$-plane. The longitudinal-phonon mode is assumed to be decoupled from transverse modes: this is valid for cubic crystals with interfaces parallel to the (100) or (111) planes. In these conditions, the elastic equation of motion of the multilayer in the direction z normal to the layers is [16, 17]

$$\rho \frac{\partial^2 u(z,t)}{\partial t^2} = \frac{\partial \sigma(z,t)}{\partial z} \tag{2}$$

where u is the lattice displacement in the direction z and σ is here the zz-component of the elastic stress tensor that is related to the displacement by

$$\sigma(z,t) = \rho v^2 \partial u/\partial z \tag{3}$$

where $\partial u/\partial z$ is the strain and $\rho(v)$ is either $\rho_A(v_A)$ or $\rho_B(v_B)$ depending on the layer considered. Looking for solutions of the form $u(z,t) = W(z)\exp(-\mathrm{i}\omega t)$ with ω a phonon angular frequency, the displacement can be written in the general form $\boldsymbol{w}(z) = (0, 0, W(z))$.

The use of the continuum model is valid for the lattice vibrations in the sub-THz range considered here, in the metallic superlattice. The continuity of the lattice displacement $u(z,t)$ and stress $\sigma(z,t)$ at the interface between any two layers leads to relations between the above solutions for the displacements in two adjacent layers that can be expressed by a 2×2 transfer matrix T. It has been shown that the matrix elements of T are functions of k_A, d_A, k_B, d_B, and Z_A and Z_B, where $k_I = \omega/v_I$ ($I = A, B$) and $Z_I = \rho_I v_I$ is the acoustic impedance. The matrix elements of the unimodular matrix T, i.e., satisfying $\det T = 1$, are [18]

$$T_{11} = \cos(k_A d_A)\cos(k_B d_B) - \frac{Z_A}{Z_B}\sin(k_A d_A)\sin(k_B d_B) \tag{4}$$

$$T_{12} = Z_A^{-1}\sin(k_A d_A)\cos(k_B d_B) + Z_B^{-1}\cos(k_A d_A)\sin(k_B d_B) \tag{5}$$

$$T_{21} = -Z_A\sin(k_A d_A)\cos(k_B d_B) - Z_B\cos(k_A d_A)\sin(k_B d_B) \tag{6}$$

$$T_{22} = \cos(k_A d_A)\cos(k_B d_B) - \frac{Z_B}{Z_A}\sin(k_A d_A)\sin(k_B d_B). \tag{7}$$

For a phonon mode propagating in an infinite superlattice the Bloch theorem requires that $\det[T - \exp(\mathrm{i}k_z D) \times U] = 0$, where k_z ($-\pi/D \leqslant k_z \leqslant \pi/D$) is a Bloch wavenumber, or superlattice wavenumber, U is the unit matrix, and $\exp(\pm\mathrm{i}k_z D)$ are the eigenvalues of T. The dispersion relation of the phonons immediately results from this relation, which was first derived by Rytov for elastic acoustic waves in stratified media with $\boldsymbol{k}_\parallel = 0$, and it takes the form [19]

$$\cos(k_z D) = \cos(k_A d_A)\cos(k_B d_B) - \frac{1}{2}\left(\frac{Z_A}{Z_B} + \frac{Z_B}{Z_A}\right)\sin(k_A d_A)\sin(k_B d_B). \tag{8}$$

This equation determines the superlattice wavenumber k_z for a given frequency ω. We assume that the modifications of the elastic parameters near the interfaces in the metallic superlattices are small enough to be neglected; we use the bulk values for the sound velocities and mass densities which are constant in each layer. As explained below, this assumption should be valid for the Al/Ag superlattice with bilayer thickness larger than about 100 Å. We note that a phonon with real wavenumber k_z is found inside a frequency band of the superlattice and we call such a phonon an extended phonon in the present paper.

On the basis of these considerations we write the quantized phonon displacement vector $\boldsymbol{u}$ in the infinite superlattices for $\boldsymbol{k}_\parallel = 0$ as [20, 21]

$$\boldsymbol{u}(\boldsymbol{x}) = \sum_J \left(\frac{\hbar}{2\omega_J S}\right)^{1/2} (a_J + a_{-J}^\dagger)\boldsymbol{w}_J(z) \tag{9}$$

where $\boldsymbol{x} = (\boldsymbol{x}_\parallel, z)$, $J = (k_z, j)$ for a phonon in a perfect, periodic superlattice with j the band index, S is the normalization area, a_J and its Hermitian conjugate $a_J^\dagger$ are the annihilation and creation operators of a phonon satisfying $[a_J, a_{J'}^\dagger] = \delta_{J,J'}$ and $\boldsymbol{w}_J(z) = (0, 0, W_J(z))$ for the longitudinal mode. Explicitly, the lattice displacement $W_J(z)$ is written as

$$W_J(z) = \sum_n e^{ink_z D}\{\Theta(z - nD)\Theta(nD + d_A - z)\rho_A^{-1/2}U_{A,J}^{(n+1)}(z) + \Theta(z - nD - d_A)\Theta[(n+1)D - z]\rho_B^{-1/2}U_{B,J}^{(n+1)}(z)\} \tag{10}$$

$$U_{A,J}^{(n+1)}(z) = \tilde{A}_{1,J}\cos[k_A(z - nD)] + \tilde{A}_{2,J}\sin[k_A(z - nD)] \tag{11}$$

$$U_{B,J}^{(n+1)}(z) = \tilde{B}_{1,J}\cos[k_B(z - nD - d_A)] + \tilde{B}_{2,J}\sin[k_B(z - nD - d_A)] \tag{12}$$

where $\Theta(z)$ is the Heaviside unit-step function ($\Theta(z) = 1$ for $z \geqslant 0$ and $\Theta(z) = 0$ for $z < 0$). The coefficients $\tilde{A}_{m,J}$ and $\tilde{B}_{m,J}$ ($m = 1, 2$) in equations (11) and (12) are determined from the boundary conditions (the continuities of the lattice displacement W_J and the associated stress) at layer interfaces and the normalization condition $\int_0^L \rho|W_J(z)|^2\,dz = 1$, where L is the normalization length (thickness of the superlattice) and ρ is either ρ_A or ρ_B depending on the position z.

3. Electron field in the Kronig–Penney model

In metal–metal contact there should occur charge transfer between adjacent materials such that the Fermi energy becomes uniform in the thermal equilibrium state. Also, charge neutrality should be satisfied locally; otherwise an electric field is set up which induces an electric current inside the system. So the difference between the intrinsic Fermi energies of the bulk metals induces the potential $V(\boldsymbol{r})$ in the system, where $V(\boldsymbol{r}) = V(z)$ ($=V_I$, where I, as before, is either A or B). Here we assume the transition region of the potential to be very narrow. Thus, as a simple approximation we may assume the Kronig–Penney model for the motion perpendicular to the layer interfaces, i.e., in the z-direction. We also assume that the metallic layers A and B have uniform mass: $m_A = m_B = m$, the free-electron mass.

The electron wavefunctions $\psi(\boldsymbol{r})$ are the solutions of the Schrödinger equation with a potential energy $V(\boldsymbol{r}) = V(z)$. Therefore, within the Kronig–Penney model with an abrupt-interface approximation, we have to solve the equation for the wavefunction $\phi_\lambda(z)$ describing the motion in the z-direction [22]:

$$\left[-\frac{\hbar^2}{2m}\frac{d^2}{dz^2} + V(z)\right]\phi_\lambda(z) = E_\lambda\phi_\lambda(z) \tag{13}$$

with the following boundary conditions: $\phi_\lambda(z)$ and the component of its derivative normal to the interface $\partial\phi_\lambda(z)/\partial z$ must be continuous across the interface separating two adjacent layers.

Along the layer interfaces, the wavefunction should be described by a plane wave, $\exp(i\boldsymbol{p}_\parallel \cdot \boldsymbol{x}_\parallel)$, with $\boldsymbol{p}_\parallel$ the two-dimensional wavevector in the $\boldsymbol{x}_\parallel$-plane. The total wavefunction $\psi(\boldsymbol{r})$ is thus $\psi(\boldsymbol{r}) = \exp(i\boldsymbol{p}_\parallel \cdot \boldsymbol{x}_\parallel) \times \phi_\lambda(z)$. The wavefunction $\phi_\lambda(z)$ takes a form similar to the expression for $W_J(z)$ with a set of quantum numbers λ instead of J, $\exp(ink_z D)$ being read here as $\exp(inp_z D)$—that is, $\lambda = (p_z, i)$ stands for the quantum numbers specifying the wavefunction $\phi_\lambda(z)$, where p_z ($-\pi/D \leqslant p_z \leqslant \pi/D$) is the Bloch wavenumber in the growth direction and i indicates a series of subbands [23]. Thus $\Lambda \equiv (\boldsymbol{p}_\parallel, \lambda) = (\boldsymbol{p}_\parallel, p_z, i)$ is the set of quantum numbers specifying the complete electron state in the superlattice and the electron energy is written as $E_\Lambda = E_{p_\parallel} + E_\lambda = \hbar^2\boldsymbol{p}_\parallel^2/2m + E_{p_z,i}$.

The explicit expression for the envelope wavefunction $\phi_\lambda(z)$ is

$$\phi_\lambda(z) = \sum_n e^{inp_z D}\{\Theta(z - nD)\Theta(nD + d_A - z)\phi_{A,\lambda}^{(n+1)}(z) + \Theta(z - nD - d_A)\Theta[(n+1)D - z]\phi_{B,\lambda}^{(n+1)}(z)\}. \tag{14}$$

Here we define V_0 as the potential height of the B-layer (the barrier layer for electrons) relative to the A-layer (the well layer for electrons), which is determined from the difference of the

Fermi energies $E_{\rm f}^A$ and $E_{\rm f}^B$ of bulk A- and B-materials, i.e., $V_0 = E_{\rm f}^A - E_{\rm f}^B > 0$. This results from the requirement that the Fermi energy $E_{\rm f}$ should be uniform in the superlattice (see figure 2). Thus, for $E_{p_z,i} > V_0$ the wavefunction in each layer of the $(n+1)$th period is [22, 24]

$$\phi_{A,\lambda}^{(n+1)}(z) = A_{1,\lambda}\cos[q_A(z-nD)] + A_{2,\lambda}\sin[q_A(z-nD)] \tag{15}$$

$$\phi_{B,\lambda}^{(n+1)}(z) = B_{1,\lambda}\cos[q_B(z-nD-d_A)] + B_{2,\lambda}\sin[q_B(z-nD-d_A)]. \tag{16}$$

In equations (15) and (16), $A_{j,\lambda}$ and $B_{j,\lambda}$ $(j = 1, 2)$ are constant coefficients and the wavenumbers q_A and q_B are defined through the energy of the electrons $E_{p_z,i} = \hbar^2 q_A^2/2m = \hbar^2 q_B^2/2m + V_0$. For $E_{p_z,i} < V_0$ the trigonometric functions $\cos[q_B(z-nD-d_A)]$ and $\sin[q_B(z-nD-d_A)]$ in equation (16) for the B-layer should be replaced with the hyperbolic functions $\cosh[q_B(z-nD-d_A)]$ and $\sinh[q_B(z-nD-d_A)]$, respectively, with q_B defined by $E_{p_z,i} = -\hbar^2 q_B^2/2m + V_0$.

Next, we introduce the transfer-matrix method [22] and write equations (15) and (16) together with their derivatives in the forms

$$\boldsymbol{\Phi}_{A,\lambda}^{(n+1)}(z) = \begin{pmatrix} \phi_{A,\lambda}^{(n+1)}(z) \\ [\phi_{A,\lambda}^{(n+1)}(z)]' \end{pmatrix} \equiv t_A(z-nD)\boldsymbol{A}_\lambda \tag{17}$$

and

$$\boldsymbol{\Phi}_{B,\lambda}^{(n+1)}(z) = \begin{pmatrix} \phi_{B,\lambda}^{(n+1)}(z) \\ [\phi_{B,\lambda}^{(n+1)}(z)]' \end{pmatrix} \equiv t_B(z-nD-d_A)\boldsymbol{B}_\lambda \tag{18}$$

where $\boldsymbol{A}_\lambda$ and $\boldsymbol{B}_\lambda$ are the column vectors given by the transpositions of $(A_{1,\lambda}, A_{2,\lambda})$ and $(B_{1,\lambda}, B_{2,\lambda})$, respectively. The 2×2 transfer matrix t for electrons relevant to the present system is then defined by $t = \tilde{t}_B\tilde{t}_A$ with $\tilde{t}_A = t_A(d_A)[t_A(0)]^{-1}$ and $\tilde{t}_B = t_B(d_B)[t_B(0)]^{-1}$. Explicitly, for $E_{p_z,i} > V_0$,

$$\tilde{t}_I = \begin{pmatrix} \cos\gamma_I & q_I^{-1}\sin\gamma_I \\ -q_I\sin\gamma_I & \cos\gamma_I \end{pmatrix} \tag{19}$$

with $I = A, B$, $\gamma_A = q_A d_A \equiv \alpha$ and $\gamma_B = q_B d_B \equiv \beta$, and for $E_{p_z,i} < V_0$, $\tilde{t}_A$ is the same as equation (19) with $I = A$ but

$$\tilde{t}_B = \begin{pmatrix} \cosh\gamma_B & q_B^{-1}\sinh\gamma_B \\ q_B\sinh\gamma_B & \cosh\gamma_B \end{pmatrix}. \tag{20}$$

Thus the elements of the transfer matrix t are

$$t_{11} = \cos\alpha\cos\beta - \frac{q_A}{q_B}\sin\alpha\sin\beta \tag{21}$$

$$t_{12} = q_A^{-1}\sin\alpha\cos\beta + q_B^{-1}\cos\alpha\sin\beta \tag{22}$$

$$t_{21} = -q_A\sin\alpha\cos\beta - q_B\cos\alpha\sin\beta \tag{23}$$

$$t_{22} = \cos\alpha\cos\beta - \frac{q_B}{q_A}\sin\alpha\sin\beta \tag{24}$$

for $E_{p_z,i} > V_0$ and

$$t_{11} = \cos\alpha\cosh\beta - \frac{q_A}{q_B}\sin\alpha\sinh\beta \tag{25}$$

$$t_{12} = q_A^{-1}\sin\alpha\cosh\beta + q_B^{-1}\cos\alpha\sinh\beta \tag{26}$$

$$t_{21} = -q_A\sin\alpha\cosh\beta + q_B\cos\alpha\sinh\beta \tag{27}$$

$$t_{22} = \cos\alpha\cosh\beta + \frac{q_B}{q_A}\sin\alpha\sinh\beta \tag{28}$$

for $E_{p_z,i} < V_0$.

The wavenumber in each layer, q_A or q_B, and the band index i are related to the superlattice wavenumber p_z of the electrons through the dispersion relation $\cos(p_z D) = (t_{11}+t_{22})/2$. This is derived from the continuity conditions of the wavefunction and its derivative at the layer interfaces, i.e., $\Phi^{(n+1)}_{A,\lambda}(nD + d_A) = \Phi^{(n+1)}_{B,\lambda}(nD + d_A)$ and $\Phi^{(n)}_{B,\lambda}(nD) = \Phi^{(n+1)}_{A,\lambda}(nD)$, and also from the Bloch theorem $\Phi^{(n+1)}_{A,\lambda}(nD) = \mathrm{e}^{\mathrm{i}p_z D}\Phi^{(n)}_{A,\lambda}[(n-1)D]$ manifesting the periodicity of the system. The explicit expression for the dispersion relation is well known and is given by [22, 24]

$$\cos(p_z D) = \cos(q_A d_A)\cos(q_B d_B) - \frac{1}{2}\left(\frac{q_A}{q_B} + \frac{q_B}{q_A}\right)\sin(q_A d_A)\sin(q_B d_B) \tag{29}$$

for $E_{p_z,i} > V_0$ and

$$\cos(p_z D) = \cos(q_A d_A)\cosh(q_B d_B) + \frac{1}{2}\left(\frac{q_B}{q_A} - \frac{q_A}{q_B}\right)\sin(q_A d_A)\sinh(q_B d_B) \tag{30}$$

for $E_{p_z,i} < V_0$. For $E_{p_z,i} > V_0$, the matrix elements in equations (21)–(24) and the dispersion relation in equation (29) are quite similar to the corresponding equations for the phonons, with q_A/q_B instead of Z_A/Z_B. The coefficients $A_{j,\lambda}$ and $B_{j,\lambda}$ ($j = 1, 2$) in equations (15) and (16) are also determined from the above-mentioned continuity and periodicity conditions for the wavefunction (and its derivative) as well as the normalization condition $\int_0^L |\phi_\lambda(z)|^2\,\mathrm{d}z = 1$.

The quantized electron field in the perfect periodic superlattice is then written as [2, 21]

$$\Psi(\boldsymbol{x}) = \sum_{\Lambda} b_\Lambda \phi_\lambda(z)\mathrm{e}^{\mathrm{i}\boldsymbol{p}_\parallel\cdot\boldsymbol{x}_\parallel}/\sqrt{S} \tag{31}$$

where b_Λ and its Hermitian conjugate $b^\dagger_\Lambda$ are the annihilation and creation operators of electrons satisfying the anticommutation relations $\{b_\Lambda, b^\dagger_{\Lambda'}\} = \delta_{\Lambda,\Lambda'}$ and $\{b_\Lambda, b_{\Lambda'}\} = 0$.

4. Electron–phonon interaction

We assume the deformation-potential coupling as the source of the electron–phonon interaction in metallic superlattices. In the Kronig–Penney model the calculated electron concentrations in the A- and B-layers coincide with those of bulk metals. This means that local charge neutrality holds in the periodic layered structure and electrons are sensitive to the local lattice vibrations. Hence for the electron–phonon coupling we employ the deformation-potential constants C_A and C_B of the bulk A- and B-metals. Thus, the interaction Hamiltonian is [2, 25]

$$\begin{aligned} H_I &= \int \mathrm{d}^3x\, \Psi^\dagger(\boldsymbol{x}) C\,\nabla\cdot\boldsymbol{u}(\boldsymbol{x})\Psi(\boldsymbol{x}) \\ &= \sum_{\Lambda',\Lambda,J}\left(\frac{\hbar}{2\omega_J S}\right)^{1/2} b^\dagger_{\Lambda'} b_\Lambda (a_J + a^\dagger_{-J})\delta_{\boldsymbol{p}'_\parallel,\boldsymbol{p}_\parallel} G(p'_z, p_z, J) F_{\lambda'\lambda J} \end{aligned} \tag{32}$$

where C is either C_A or C_B depending on the position z. The expression for $F_{\lambda'\lambda J}$ is

$$F_{\lambda'\lambda J} = \frac{C_A}{\rho_A^{1/2}}\int_0^{d_A} \mathrm{d}z\,\phi^*_{A,\lambda'}(z)\frac{\mathrm{d}U_{A,J}(z)}{\mathrm{d}z}\phi_{A,\lambda}(z) + \frac{C_B}{\rho_B^{1/2}}\int_0^{d_B}\mathrm{d}z\,\phi^*_{B,\lambda'}(z)\frac{\mathrm{d}U_{B,J}(z)}{\mathrm{d}z}\phi_{B,\lambda}(z) \tag{33}$$

where $\phi_{A,\lambda}(z) = \phi^{(1)}_{A,\lambda}(z)$, $\phi_{B,\lambda}(z) = \phi^{(1)}_{B,\lambda}(z+d_A)$, $U_{A,J}(z) = U^{(1)}_{A,J}(z)$, and $U_{B,J}(z) = U^{(1)}_{B,J}(z+d_A)$. The integrations of equation (33) can be done analytically with equations (11), (12), (15), and (16). The results are lengthy and so are given in the appendix. Also in equation (32) G takes the form [22]

$$G(p'_z, p_z, J) = G(p'_z, p_z, k_z) = N\Delta(p'_z - p_z - k_z) \tag{34}$$

where N is the number of periods, $\Delta(p_z) = 1$ if p_z is a reciprocal-superlattice vector and $\Delta(p_z) = 0$ otherwise. This form of G shows the conservation of the superlattice wavenumbers.

5. Attenuation rates

For comparison with the Pippard formula for bulk metals [1], we consider the attenuation rate of the bulk phonons in a perfect, periodic superlattice. Just like in the case for the bulk metals [1,24], the interaction between an electron and a phonon is assumed to be weak enough for their respective states to be relatively long lived so that the first-order perturbation theory can be used to calculate the scattering rate. Thus, applying the golden rule for the transition rate, we can derive the equation for the deviation Δn_J of the phonon occupation number n_J from the thermal equilibrium value:

$$-\frac{\Delta \dot{n}_J}{\Delta n_J} = \tau_J^{-1} = \frac{2\pi}{\omega_J S} \sum_{\Lambda',\Lambda} |G(p_z', p_z, J)|^2 |F_{\lambda'\lambda J}|^2 (f_\Lambda - f_{\Lambda'}) \delta_{\boldsymbol{p}_\parallel', \boldsymbol{p}_\parallel} \delta(E_{\Lambda'} - E_\Lambda - \hbar\omega_J) \tag{35}$$

where f_Λ is the electron occupation number. We again emphasize that we have considered the phonon with $\boldsymbol{k}_\parallel = 0$, i.e., a phonon in a frequency band propagating normal to the layer interfaces. Note that τ_J corresponds to the energy relaxation time and we refer to τ_J^{-1} as the attenuation rate of the J-phonon.

Here we remark that the electron energy $E_{p_z,i}$ in the perfect Kronig–Penney system depends implicitly on the wavenumber p_z and band index i through the dispersion relation (29) or (30). Comparing with the case of the electron–phonon interaction in a bulk material, these situations make it rather onerous to complete the calculation of the relaxation time. Explicitly, the procedure for the calculation of equation (35) is as follows: for given ω and k_z, first we determine the wavenumbers and energies $(p_z, E_{p_z,i})$ and $(p_z', E_{p_z',i'})$ which satisfy the energy and superlattice wavenumber conservation $E_{p_z',i'} - E_{p_z,i} - \hbar\omega_J = E_{p_z+k_z+g,i'} - E_{p_z,i} - \hbar\omega_J = 0$, where g is a reciprocal-superlattice wavenumber. In general, there exist several sets of initial wavenumbers and energies $(p_z, E_{p_z,i}) = (p_z^{(n)}, E^{(n)})$ $(n = 1, 2, \ldots)$ satisfying the above equation. This is a characteristic feature associated with the folded band structure of electrons.

We further note the fact that at a temperature much lower than the Fermi temperature, the factor $f_\Lambda - f_{\Lambda'}$ is unity for $E_\mathrm{f} - \hbar\omega_J - E_{p_z,i} < E_{\boldsymbol{p}_\parallel} < E_\mathrm{f} - E_{p_z,i}$ and zero otherwise, and also $\sum_\Lambda = \sum_{\boldsymbol{p}_\parallel,\lambda} = [V/(2\pi)^3] \int \mathrm{d}^2 p_\parallel \int_{-\pi/D}^{\pi/D} \mathrm{d}p_z \sum_i$. Thus the integral over $\boldsymbol{p}_\parallel$ in equation (35) gives a factor $2\pi m\omega_J/\hbar$ and it is readily derived:

$$\tau_J^{-1} = \frac{LN^2}{2\pi} \frac{m}{\hbar} \sum_n |F_{\lambda'\lambda J}|^2 \left| \frac{\mathrm{d}E_{p_z,i}}{\mathrm{d}p_z} - \frac{\mathrm{d}E_{p_z+k_z+g,i'}}{\mathrm{d}p_z} \right|^{-1}_{p_z^{(n)}, E^{(n)}} \tag{36}$$

where $|_{p_z^{(n)}, E^{(n)}}$ means $(p_z, E_{p_z,i})$ should be equal to $(p_z^{(n)}, E^{(n)})$. Here we note that the energy $E_{p_z,i}$ is not restricted to a value close to the Fermi energy E_f because of the presence of the energy $E_{\boldsymbol{p}_\parallel}$, and hence $E^{(n)}$ can be any value between 0 and E_f.

Equation (36) is the attenuation rate for the phonons (with $\boldsymbol{k}_\parallel = 0$) in superlattices to be used for the numerical calculations. In the case where the A- and B-layers consist of the same material, there exists only one p_z satisfying $\mathrm{d}E_{p_z,i}/\mathrm{d}p_z - \mathrm{d}E_{p_z+k_z+g,i'}/\mathrm{d}p_z = (\hbar^2/m)(p_z - p_z') = -\hbar^2 k_z/m$ and we have $F_{\lambda'\lambda J} = Ck_z D(\rho L^3)^{-1/2}$ with $C_A = C_B = C$, $\rho_A = \rho_B = \rho$, and $L = ND$. Thus, equation (36) is reduced to

$$\tau_J^{-1} = \frac{C^2 m^2 k_z}{2\pi\rho\hbar^3}. \tag{37}$$

Because we are considering phonons propagating in the z-direction, this expression for the attenuation rate coincides with the Pippard formula, equation (1), for the attenuation of high-frequency longitudinal phonons (satisfying $k_z l_\mathrm{e} \gg 1$, with l_e the electron mean free path) in a bulk metal.

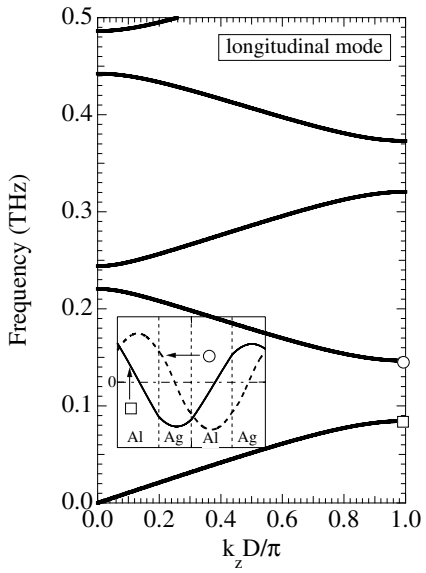

Figure 1. The dispersion relation of longitudinal phonons propagating normal to the layer interfaces of the Al/Ag superlattice with $d_A = d_{\mathrm{Al}} = 121$ Å and $d_B = d_{\mathrm{Ag}} = 97$ Å ($D = d_A + d_B = 218$ Å). The inset shows the lattice displacements in the superlattice at the lower edge (solid curve) and the upper edge (dashed curve) of the lowest-frequency gap marked with the open square and circle, respectively.

6. Numerical calculations

Now we apply the formulae (36) to the calculation of the attenuation rates of the longitudinal phonons in an Al/Ag superlattice with $d_A = d_{\mathrm{Al}} = 121$ Å and $d_B = d_{\mathrm{Ag}} = 97$ Å ($D = 218$ Å). These layer thicknesses are the same as those of the superlattice used for the picosecond ultrasound experiment by Chen *et al* [15]. We also assume other parameters assumed by Chen *et al* to analyse phonon properties in Al/Ag superlattices: $\rho_A = \rho_{\mathrm{Al}} = 2.7$ g cm^{-3}, $\rho_B = \rho_{\mathrm{Ag}} = 10.5\,\mathrm{g\,cm^{-3}}$, $v_A = v_{\mathrm{Al}} = 6.4\times10^5\,\mathrm{cm\,s^{-1}}$, and $v_B = v_{\mathrm{Ag}} = 4.0\times10^5\,\mathrm{cm\,s^{-1}}$ [15]. The Fermi energies of electrons in aluminium and silver are 11.63 and 5.48 eV, respectively, and the difference of these values gives $V_0 = 6.15$ eV for the potential barrier height in the Kronig–Penney model. The deformation-potential constants are calculated from the Fermi energies of silver and aluminium as $C_A = C_{\mathrm{Al}} = -7.57$ eV and $C_B = C_{\mathrm{Ag}} = -3.65$ eV.

6.1. Dispersion relations

Figure 1 shows the calculated dispersion relation (together with the displacement profiles at the lowest zone-boundary frequencies) of the longitudinal phonons propagating along the growth direction of the Al/Ag superlattice. Because of the large acoustic mismatch between the constituent materials ($Z_{\mathrm{Ag}}/Z_{\mathrm{Al}} = 2.43$) the widths of the frequency gaps (∼50 GHz) are considerable compared with the bandwidths (∼100 GHz).

Figure 2 shows the dispersion relation of electrons calculated from the Kronig–Penney model together with a schematic diagram of the energy profile for the electrons. Because of the large thickness ($d_B = d_{\mathrm{Ag}} = 97$ Å) of the potential barrier (silver layer) for electrons, the bandwidths are negligibly small at energies below V_0, leading to discrete energy levels for $E_{p_z,i} < V_0$. Energy bands of sizable width are found only for $E_{p_z,i} > V_0$. In the superlattice

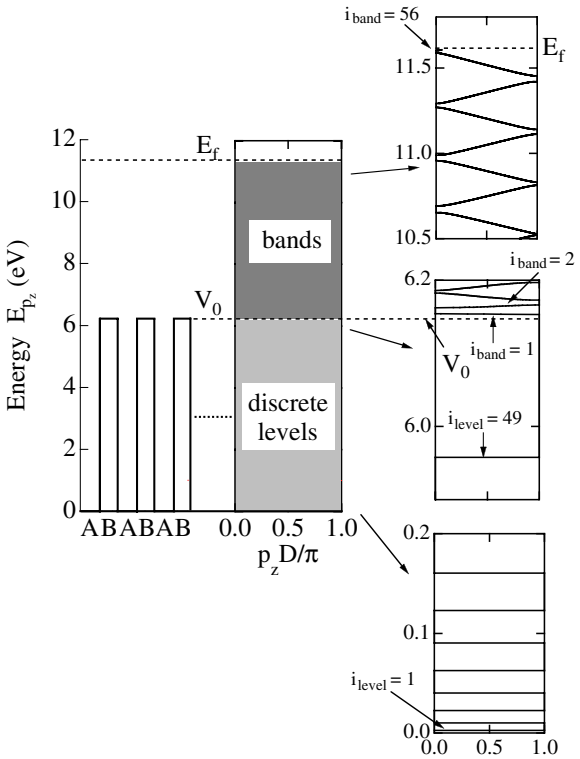

Figure 2. A schematic energy diagram (on the left-hand side) of the conduction band for electrons and the dispersion relations (E_{p_z} versus p_z) of electrons (on the right-hand side) in the perfect, periodic Al/Ag superlattice (A = Al, B = Ag) with $d_A = d_{\mathrm{Al}} = 121$ Å and $d_B = d_{\mathrm{Ag}} = 97$ Å ($D = d_A + d_B = 218$ Å). Enlarged views of the three energy regions near the bottom, $E_{p_z} = 0$, $E_{p_z} = V_0$, and the top, $E_{p_z} = E_{\mathrm{f}}$, are shown. The Fermi energy and potential height are $E_{\mathrm{f}} = 11.63$ eV and $V_0 = 6.15$ eV, respectively.

considered, the number of these discrete levels below V_0 is 49, i.e., $i = i_{\mathrm{level}} = 1$–49, and the smallest energy difference among these levels is much larger than the phonon energy of frequency 1 THz (4.1 meV). The number of energy bands between V_0 and the Fermi energy $E_{\mathrm{f}} = 11.63$ eV is 56, i.e., $i_{\mathrm{band}} = 1$–56, and for these electron bands the band indices are assigned as $i = i_{\mathrm{band}} + 49 = 50$–105. No interband transition is allowed, for electrons, by the absorption or emission of a single sub-THz phonon that we consider.

6.2. Attenuation rate of phonons

The attenuation rates of the extended phonons in the superlattice calculated with the parameters assumed above are shown in figure 3. In the lowest-frequency band of phonons the attenuation rate increases linearly with frequency except near the zone boundary. In this region the magnitude is about half of the attenuation rate for the bulk phonons in aluminium, $\tau_{\mathrm{Al}}^{-1} = 6.0 \times 10^{-2} \nu\ \mathrm{s}^{-1}$, obtained from the Pippard formula, equation (1), and larger than the attenuation rate in bulk silver, $\tau_{\mathrm{Ag}}^{-1} = 5.67 \times 10^{-3} \nu\ \mathrm{s}^{-1}$. However, as explained below, the attenuation rate τ_j^{-1} in the low-frequency region is not simply the average of τ_{Al}^{-1} and τ_{Ag}^{-1} for the bulk metals weighted by the relative thickness of the layers.

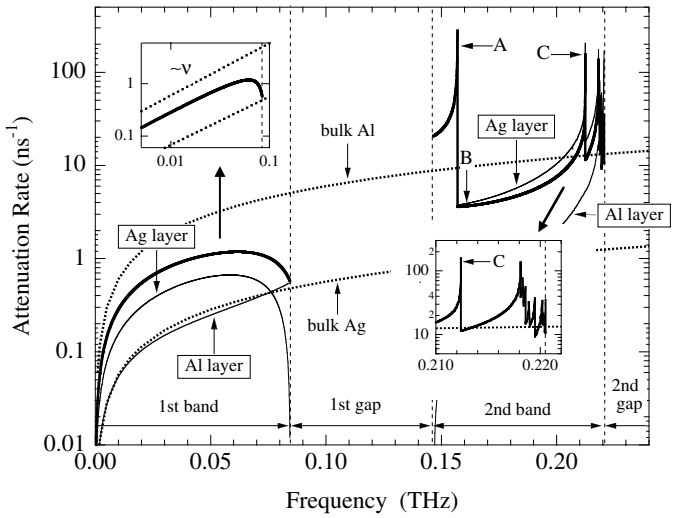

Figure 3. Attenuation rates (bold solid curves) of the longitudinal phonon propagating along the growth direction of the Al/Ag superlattice with $D = 218$ Å. Thin solid curves show the contributions from the interactions in the Al and Ag layers. The attenuation rates (Pippard's formula, equation (1)) for the bulk aluminium and silver are shown by dotted curves. Insets show a log–log plot of the attenuation rate in the low-frequency region and also an enlarged view of the attenuation rate (bold curve) near the upper edge of the second frequency band.

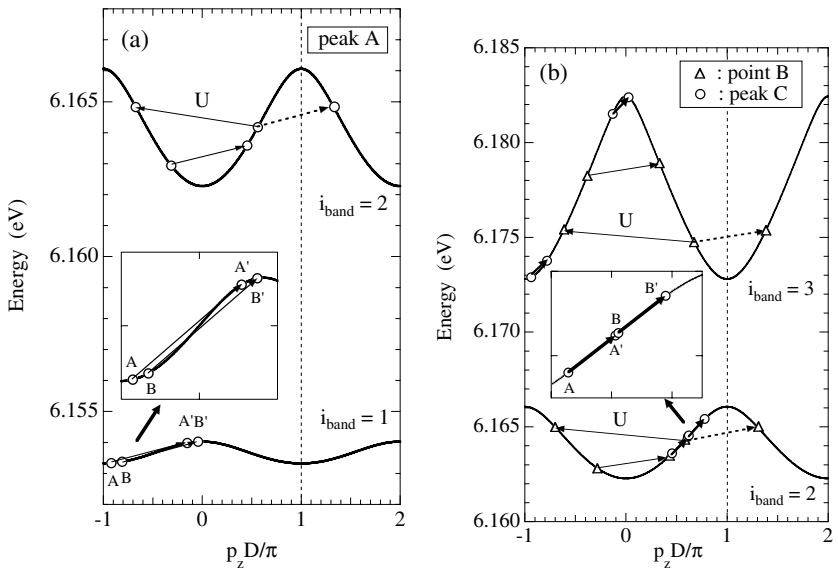

Figure 4. Scattering processes of the extended phonons in the low-lying electron bands contributing to (a) peak A at $\nu = 0.156$ THz of figure 3, (b) point B at $\nu = 0.16$ THz (thin arrows) and peak C at $\nu = 0.212$ THz (bold arrows) of figure 3. The processes labelled 'U' are the Umklapp scatterings and the dashed curves are the corresponding original processes scattered outside the folded Brillouin zone. Insets show enlarged views of the processes contributing to the enhanced scatterings at the peaks A and C.

The decrease of the attenuation rate near the zone boundary is due to the fact that the interaction in the Ag layer becomes small. As shown in the inset of figure 1, at the lower edge of the lowest-frequency gap, the boundaries of the heavier Ag layer vibrate in the same direction but those of the lighter Al layer vibrate in opposite directions. This means that the volume change which induces the scattering of electrons occurs predominantly in the Al layer.

Actually the electron–phonon interaction in the Al/Ag superlattice is stronger in the Ag layer except near the zone-centre or zone-boundary frequencies for which the volume change in this layer does not occur. This is quite different from the naive expectation by Chen *et al* [15] that a larger damping occurs in superlattices that contain a larger volume of Al than of Ag. The reason is as follows: first we consider an electron in the first band $i_{\text{band}} = 1$ with an energy slightly above the edge of the potential barrier V_0, or $E_{p_z,i} \simeq V_0 + 0.01$ eV, for example. The corresponding wavenumbers are $q_A = q_{\text{Al}} \simeq 1 \times 10^8$ cm^{-1} (a well region) and $q_B = q_{\text{Ag}} \simeq 5 \times 10^6$ cm^{-1} (a barrier region). On the other hand, in the sub-THz region the wavenumbers of a phonon which interacts with electrons are $k_A, k_B \simeq 1 \times 10^6$ cm^{-1}. Accordingly, the order of magnitude of the electron wavenumber in each layer does not change by the emission or absorption of a phonon. This means that the electron wavefunctions $\phi_{A,\lambda}$ and $\phi^*_{A,\lambda'}$ oscillate much faster than $\phi_{B,\lambda}$ and $\phi^*_{B,\lambda'}$, and hence the integral in $F_{\lambda'\lambda J}$ (equation (33)) over the layer thickness ($d_A, d_B \approx 10^{-6}$ cm^{-1}) is much smaller in the Al (A-) layer than in the Ag (B-) layer.

At higher electron energies, e.g., $E_{p_z,i} - V_0 \sim 1$ eV, both q_B and q_A are of the order of 1×10^8 cm^{-1} and the integrals in equation (33) give comparable magnitudes—but small compared with the contribution from $E_{p_z,i} \sim V_0$. These results can also be understood from the analytical expressions for the overlapping integrals given in the appendix. The combined effects of the deformation-potential constants and the integrals in $F_{\lambda'\lambda J}$ result in dominant electron–phonon scattering in the Ag layer (the barrier layer for electrons), in spite of the fact that $|C_{\text{Al}}| \approx 2|C_{\text{Ag}}|$ and $d_{\text{Al}} > d_{\text{Ag}}$.

A more interesting result is the fact that the attenuation rate exhibits spiky resonant structures for phonons in the higher bands, as shown in figure 3 for the second frequency band of phonons. These resonant structures arise from the Brillouin-zone folding of the periodic superlattice and the associated deformation of the dispersion curves of both electrons and phonons. To show this, we have illustrated in figures 4(a) and (b) several energy–momentum-conserving processes which scatter the phonons of frequencies 0.156, 0.16, and 0.212 THz. Note that the scattering is enhanced at the first and third frequencies, but no enhancement is predicted at the second frequency.

The enhanced attenuation at 0.156 THz (the peak labelled A in figure 3) comes from the two absorption processes, A to A′ and B to B′, that occurred in the lowest electron band above V_0, or $i_{\text{band}} = 1$ (figure 4(a)) and also from the corresponding emission processes. In these processes both the initial (A or B) and scattered (A′ or B′) electron states exist in the same band and the region $p_z < 0$ of the mini-zone. Thus, the slopes of the dispersion curve for those states have the same sign and their magnitudes are nearly equal. This means that there exist a large number of initial and final electron states that can absorb or emit a given phonon. Mathematically, the denominator $|\mathrm{d}E_{p_z,i}/\mathrm{d}p_z - \mathrm{d}E_{p_z+k_z+g,i'}/\mathrm{d}p_z|$ of equation (36) becomes very small for $i = i' = 50$, or $i_{\text{band}} = i'_{\text{band}} = 1$, leading to the resonant peak of τ_J^{-1} at 0.156 THz.

However, for other scattering processes in the band $i_{\text{band}} = 2$ shown in figure 4(a) the slopes of the dispersion curves for the initial and final electron states have different signs. Hence $|\mathrm{d}E_{p_z,i}/\mathrm{d}p_z - \mathrm{d}E_{p_z+k_z+g,i'}/\mathrm{d}p_z|$ for $i = i' = 51$, or $i_{\text{band}} = i'_{\text{band}} = 2$, does not become so small and no large enhancement in the scattering is produced. As the phonon frequency increases, the scattering processes for which the slopes of the dispersion curves at the initial

and final electron states are close to each other move towards higher bands of electrons. This effect is the origin of the enhanced scatterings found at higher phonon frequencies. Figure 4(b) explains why the peak C originates from the scattering processes in the band $i_{\text{band}} = i'_{\text{band}} = 3$ but no such processes contribute to the enhanced attenuation that is found for the point B.

7. Concluding remarks

Stimulated by the experiment by Chen *et al* [15], we have considered the correction to the Pippard theory of the electron–phonon interaction in multilayered structures, or superlattices. We found that the calculated attenuation rate of phonons in metallic superlattices exhibits a monotonic frequency dependence only at low frequencies in the lowest-frequency band of phonons. For these frequencies the magnitude of the attenuation rate is comparable to the one estimated from the simple application of the Pippard theory to bulk metals.

In higher bands of phonons, however, the attenuation rate is predicted to show spiky enhanced structures. These peaks in attenuation are the resonances due to the folded band structures of electrons and phonons characteristic of a periodic system. Unfortunately, however, measurement of the damping rate of the extended phonons in metallic superlattices has not yet been reported.

An interesting observation is the fact that the attenuation in the Al/Ag superlattice occurs predominantly in the Ag layer (the barrier layer for electrons). This is a quite unexpected result because the attenuation of phonons in bulk Al is about a factor of 10 larger than that in bulk Ag. This is caused by the band structure of electrons in the superlattice composed of Al and Ag layers.

Here it should be remarked that the sound velocity is modified by the electron–phonon interaction. For bulk metals this effect was calculated by Steinberg [26]. According to his result the modification of the sound velocity v due to electrons is small and the correction $\delta v/v$ is of the order of 10^{-4} to 10^{-5} at frequency 100 GHz. In metallic superlattices the sound velocity change may also be enhanced, like the experimental attenuation rates. However, it should still be small even if an order-of-magnitude enhancement occurs in the superlattices. Hence, we have neglected this effect in the calculation of the attenuation rates via the electron–phonon interaction.

Finally, we remark that the result that we obtained should also be valid for the attenuation of extended phonons in a semi-infinite superlattice. The reason is that the presence of the free surface in the superlattice does not effectively change the scattering rate for the extended phonons. This is because the electron–phonon matrix element in the perfect, periodic superlattice deviates from the one in the semi-infinite superlattice by an amount of the order of the ratio of the volume of a single bilayer to that of the entire superlattice. This ratio should be vanishingly small for a semi-infinite superlattice with many periods. (Although the surface electronic states appear in a semi-infinite superlattice in general [27], the continuous energy spectrum of the extended electrons is essentially the same as the one in the allowed energy band of the perfect, periodic superlattice.) This is because the energies of electrons of the infinite (perfect periodic) and semi-infinite periodic systems are both determined from the eigenvalues of the transfer matrix t which connects the wavefunctions and their derivatives for adjacent periods, and are insensitive to the boundary conditions [28].

Acknowledgments

One of the authors (ST) acknowledges H Akera for valuable discussions. He would also like to thank Université Pierre et Marie Curie (Paris VI) and Ecole Normale Superieure for hospitality.

This work was supported in part by the Université Pierre et Marie Curie and by a Grant-in-Aid for Scientific Research from the Ministry of Education, Science and Culture of Japan (Grant number 12640304).

Appendix

In this appendix we give the explicit expression for the first integral of equation (33). The second part is obtained by replacing A by B.

$$\begin{aligned}
&\int_0^{d_A} \mathrm{d}z\, \phi^*_{A,\lambda'}(z)\frac{\mathrm{d}U_{A,J}(z)}{\mathrm{d}z}\phi_{A,\lambda}(z)\\
&\quad= \frac{k_A}{\mathrm{i}(q'_A+q_A+k_A)}\big\{(\hat{X}_{\lambda'}X_\lambda\tilde{X}_J-\hat{Y}_{\lambda'}Y_\lambda\tilde{Y}_J)\{\cos[(q'_A+q_A+k_A)d_A]-1\}\\
&\quad+\mathrm{i}(\hat{X}_{\lambda'}X_\lambda\tilde{X}_J+\hat{Y}_{\lambda'}Y_\lambda\tilde{Y}_J)\sin[(q'_A+q_A+k_A)d_A]\big\}\\
&\quad+\frac{k_A}{\mathrm{i}(q'_A+q_A-k_A)}\big\{(\hat{X}_{\lambda'}X_\lambda\tilde{Y}_J-\hat{Y}_{\lambda'}Y_\lambda\tilde{X}_J)\{\cos[(q'_A+q_A-k_A)d_A]-1\}\\
&\quad+\mathrm{i}(\hat{X}_{\lambda'}X_\lambda\tilde{Y}_J+\hat{Y}_{\lambda'}Y_\lambda\tilde{X}_J)\sin[(q'_A+q_A-k_A)d_A]\big\}\\
&\quad+\frac{k_A}{\mathrm{i}(q'_A-q_A+k_A)}\big\{(\hat{X}_{\lambda'}Y_\lambda\tilde{X}_J-\hat{Y}_{\lambda'}X_\lambda\tilde{Y}_J)\{\cos[(q'_A-q_A+k_A)d_A]-1\}\\
&\quad+\mathrm{i}(\hat{X}_{\lambda'}Y_\lambda\tilde{X}_J+\hat{Y}_{\lambda'}X_\lambda\tilde{Y}_J)\sin[(q'_A-q_A+k_A)d_A]\big\}\\
&\quad+\frac{k_A}{\mathrm{i}(q'_A-q_A-k_A)}\big\{(\hat{X}_{\lambda'}Y_\lambda\tilde{Y}_J-\hat{Y}_{\lambda'}X_\lambda\tilde{X}_J)\{\cos[(q'_A-q_A-k_A)d_A]-1\}\\
&\quad+\mathrm{i}(\hat{X}_{\lambda'}Y_\lambda\tilde{Y}_J+\hat{Y}_{\lambda'}X_\lambda\tilde{X}_J)\sin[(q'_A-q_A-k_A)d_A]\big\} \qquad (A.1)
\end{aligned}$$

where $\tilde{X}_J=\tilde{A}_{2,J}+\mathrm{i}\tilde{A}_{1,J}$, $\tilde{Y}_J=\tilde{A}_{2,J}-\mathrm{i}\tilde{A}_{1,J}$, $X_\lambda=A_{1,\lambda}-\mathrm{i}A_{2,\lambda}$, $Y_\lambda=A_{1,\lambda}+\mathrm{i}A_{2,\lambda}$, $\hat{X}_\lambda=A^*_{1,\lambda}-\mathrm{i}A^*_{2,\lambda}$, and $\hat{Y}_\lambda=A^*_{1,\lambda}+\mathrm{i}A^*_{2,\lambda}$. We note that only the terms involving $q'_A-q_A-k_A$ are finite in the limit of $A=B$, i.e. for a bulk metal.

References

[1] Pippard A B 1960 *Proc. R. Soc.* A **257** 165
[2] See also Tucker J W and Rampton V W 1972 *Microwave Ultrasonics in Solid State Physics* (Amsterdam: North-Holland)
[3] Hepfer K C and Rayne A 1971 *Phys. Rev.* B **4** 1050
[4] Barker S Jr, Merz J L and Gossard A C 1978 *Phys. Rev.* B **17** 3181
[5] Narayanamurti V, Störmer H L, Chin M A, Gossard A C and Wiegmann W 1979 *Phys. Rev. Lett.* **43** 2012
[6] Colvard C, Merlin R, Klein M V and Gossard A C 1980 *Phys. Rev. Lett.* **45** 298
Colvard C, Gant T A, Klein M V, Merlin R, Fischer R, Morkoc H and Gossard A C 1985 *Phys. Rev.* B **31** 2080
[7] Jusserand B, Paquet D and Regreny A 1984 *Phys. Rev.* B **30** 6245
[8] Camley R E, Djafari-Rouhani B, Dobrzynski L and Maradudin A A 1983 *Phys. Rev.* B **27** 7318
[9] Sapriel J, Djafari-Rouhani B and Dobrzynski L 1983 *Surf. Sci.* **126** 197
[10] Djafari-Rouhani B, Dobrzynski L, Duparc O H, Camley R E and Maradudin A A 1983 *Phys. Rev.* B **28** 1711
[11] Dobrzynski L, Djafari-Rouhani B and Duparc O H 1984 *Phys. Rev.* B **29** 3138
[12] Grahn H T, Maris H J, Tauc J and Abeles B 1988 *Phys. Rev.* B **38** 6066
[13] El Boudouti E H, Djafari-Rouhani B and Nougaoui A 1995 *Phys. Rev.* B **51** 13 801
[14] Mizuno S and Tamura S 1996 *Phys. Rev.* B **53** 4549
[15] Chen W, Lu Y, Maris H J and Xiao G 1994 *Phys. Rev.* B **50** 14 506
[16] Brekhovskikh L M 1960 *Waves in Layered Media* (New York: Academic)
[17] Ewing W M, Jardetzky W S and Press F 1957 *Elastic Waves in Layered Media* (New York: McGraw-Hill)
[18] See, for example, Mizuno S and Tamura S 1992 *Phys. Rev.* B **45** 734

[19] Rytov S M 1956 *Akust. Zh.* **2** 71 (Engl. transl. 1956 *Sov. Phys.–Acoust.* **2** 68)
[20] Maradudin A A 1969 *Elementary Excitations in Solids* (New York: Plenum) ch 1
[21] Kittel C 1963 *Quantum Theory of Solids* (New York: Wiley) ch 1
[22] Ivchenko E L and Pikus G E 1997 *Superlattices and Other Heterostructures* 2nd edn (New York: Springer)
[23] Burt M G 1988 *Semicond. Sci. Technol.* **3** 739
Burt M G 1988 *Semicond. Sci. Technol.* **3** 1224
Burt M G 1992 *J. Phys.: Condens. Matter* **4** 6651
[24] Ridley B K 1997 *Electrons and Phonons in Semiconductor Multilayers* (Cambridge: Cambridge University Press)
[25] Abrikosov A A, Gorkov L P and Dzyaloshinski E 1975 *Methods of Quantum Field Theory in Statistical Physics* (New York: Dover) ch 2
[26] Steinberg M S 1958 *Phys. Rev.* **111** 425
See also, Truell R, Elbaum C and Chick B B 1969 *Ultrasonic Methods in Solid State Physics* (New York: Academic)
[27] Djafari-Rouhani B, Dobrzynski L and Masri P 1985 *Phys. Rev.* B **31** 7739
[28] Ledermann W 1944 *Proc. R. Soc.* A **182** 362
See, also, Maradudin A A, Montroll E W, Weiss G H and Ipatova I P 1971 *Solid State Physics (suppl.)* vol 3 (New York: Academic)